

## Coherent Phonon Assisted Ultrafast Order-Parameter Reversal and Hidden Metallic State in Ta<sub>2</sub>NiSe<sub>5</sub>


Mengxue Guan<sup>1,2</sup>, Daqiang Chen,<sup>2,3</sup> Qing Chen,<sup>2,3</sup> Yugui Yao,<sup>1,\*</sup> and Sheng Meng<sup>2,3,4,†</sup>

<sup>1</sup>*Centre for Quantum Physics, Key Laboratory of Advanced Optoelectronic Quantum Architecture and Measurement (Ministry of Education), School of Physics, Beijing Institute of Technology, Beijing 100081, China*

<sup>2</sup>*Beijing National Laboratory for Condensed Matter Physics and Institute of Physics, Chinese Academy of Sciences, Beijing 100190, China*

<sup>3</sup>*School of Physical Sciences, University of Chinese Academy of Sciences, Beijing 100190, China*

<sup>4</sup>*Songshan Lake Materials Laboratory, Dongguan, Guangdong 523808, China*

 (Received 22 June 2023; revised 20 November 2023; accepted 1 December 2023; published 21 December 2023)

The nonequilibrium dynamics during photoinduced insulator-to-metal transition (IMT) in the excitonic insulator (EI) candidate Ta<sub>2</sub>NiSe<sub>5</sub> have been investigated, which reproduce the timescale and spectral features of the ultrafast switch and reveal intricate many-body interactions involving multidegrees of freedom. The key role of lattice order parameter (OP) reversal, occurring on a timescale comparable to that of purely electronic processes (<100 fs), is identified. This reversal is enabled by the anharmonic interactions between EI-OP-coupled phonons and the conventional coherent phonons, leading to a modified potential energy landscape and a high-frequency mode up-conversion. The phonon excitation depends on the dynamics of photocarriers distributed around the Fermi level, and thus intertwines with the excitonic quenching and the complete gap collapse. These findings provide a comprehensive understanding of exciton-phonon dynamics in correlated quantum materials.

DOI: [10.1103/PhysRevLett.131.256503](https://doi.org/10.1103/PhysRevLett.131.256503)

Ta<sub>2</sub>NiSe<sub>5</sub> is widely recognized as one of the most promising materials for hosting a ground state resembling a Bose-Einstein condensation (BEC) of excitons, forming a so-called excitonic insulator (EI) state [1–4]. Below the critical temperature  $T_c \approx 328$  K, the top of highest valence bands undergoes an unusual flattening, accompanied by the opening of a narrow band gap ( $\Delta \approx 0.16$  eV) due to the hybridization between the electron and hole (e-h) pockets [2–5]. However, the notion that the gap opening is solely driven by excitonic effects (i.e., triggered by the electron-hole Coulomb interaction) is challenged by the simultaneous occurrence of an orthorhombic-to-monoclinic lattice distortion [5–12]. The lattice instability may also contribute to the gap formation via electron-phonon couplings (EPC) [12–18]. Consequently, a quantitative inquiry arises to determine the respective contributions of electronic and structural instabilities in determining the formation of the EI state. This investigation is complicated by the linearly coupled order parameters between the electronic and lattice subsystems, which lack a symmetry distinction [5–9,13,18–21].

Ultrafast methods, such as time- and angle-resolved photoemission spectroscopy (tr-ARPES) and transient absorption, have emerged as powerful tools for elucidating the microscopic origin of gap opening and manipulating the state of matter in Ta<sub>2</sub>NiSe<sub>5</sub>. By tracking the nonequilibrium evolution of the gap size, these techniques have successfully captured the insulator-to-metal transition (IMT) [8,12,14,17,22–28]. However, due to variations in the laser

parameters, controversial results regarding the underlying mechanisms have been reported. For example, due to the ultrafast metallization within 100 fs, some studies claimed that the gap collapse under strong-field excitation (laser fluence  $F > 1$  mJ/cm<sup>2</sup>) is attributed to plasma-induced screening of excitonic correlations, suggesting a purely electronic process [29–31]. In contrast, recent tr-ARPES observations suggest that the maximum gap response occurs on a phononic timescale ( $\sim 300$  fs,  $F < 0.85$  mJ/cm<sup>2</sup>), indicating a predominantly structural character [17]. Therefore, it is crucial to establish a comprehensive understanding of the entangled electron-lattice dynamics and reconcile conflicting outcomes, both for fundamental understanding and practical applications of ultrafast optical switches.

Here, we report the leading contribution of structural distortion in inducing the instability of the EI phase and the emergence of a hidden metallic state. The ultrafast IMT is enabled by the strong displacive excitation of an optical phonon with a frequency of 3 THz. Although this phonon is not directly involved in the formation of the EI state, its anharmonic interactions with the EI-OP-coupled phonon ( $\sim 2$  THz) give rise to a combined high-frequency phonon mode and a modulated potential energy surface (PES). The reshaped PES facilitates the reversal of lattice order parameter (OP), leading to an accelerated IMT with a time constant being approximately inverse dependent on the laser amplitude  $E_0(F^{0.5})$ . This process competes with purely electronic processes, particularly under intense laser

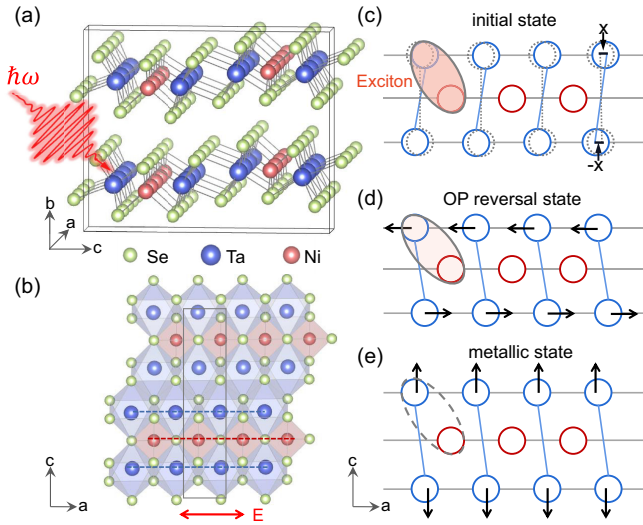


FIG. 1. (a),(b) Crystal structure of  $\text{Ta}_2\text{NiSe}_5$  viewed along two axes. The dashed lines indicate the 1D Ta and Ni chains along the  $a$  axis. (c) Schematic illustration of lattice distortion between the monoclinic (colored) and orthorhombic (gray dashed) lattice, the OP of lattice subsystem ( $X = 1$ ) is defined as the shear displacements of Ta chains accompanied by the symmetry breaking, as labeled by the black arrows. In real space, an exciton is formed between an electron on the Ta chain and a hole on the Ni chain. (d),(e) Atomic configurations of the OP inverted state ( $X = -1$ ,  $Q_{3\text{ THz}} = 0$ ) and the long-lived metallic state ( $X = -1$ ,  $Q_{3\text{ THz}} \neq 0$ ), which lead to weakened and completely quenched excitonic effects.

excitation. The phonon coupling is closely related to the dynamics of photocarriers distributed around the Fermi energy ( $E_F$ ). As a result, the change of lattice structure intertwines with the nonequilibrium excitonic effects, potentially leading to the complete quenching of excitonic condensation.

$\text{Ta}_2\text{NiSe}_5$  possesses a layered structure, where the layers are loosely held together by van der Waals' forces along the  $b$  axis. Each layer is composed of parallel chains of  $\text{TaSe}_6$  octahedra and  $\text{NiSe}_4$  tetrahedra, aligned along the crystallographic  $a$  axis [Figs. 1(a) and 1(b)]. The quasi-one-dimensional (1D) nature of  $\text{Ta}_2\text{NiSe}_5$  gives rise to the observed flattening of the valence band below  $T_c$  [2,3,26]. In the electronic subsystem, the OP corresponds to the collective hopping of electrons and holes between the Ta and Ni chains, with their spatial separation preventing excitonic states from undergoing recombination. As for the lattice subsystem, its OP associated with the EI formation can be defined as the atomic displacements of Ta chains along the  $a$  axis (referred to as  $X$  hereafter), when the lattice symmetry is lowered from the orthorhombic phase to the monoclinic phase [5] [Fig. 1(c)]. This specific shear motion follows the similar eigenvector of the  $B_{2g}$  zone-center optical phonon, which exhibits the most prominent features of the structural phase transition [9,10,24].

To investigate these phenomena further, real-time time-dependent density functional theory molecular dynamics

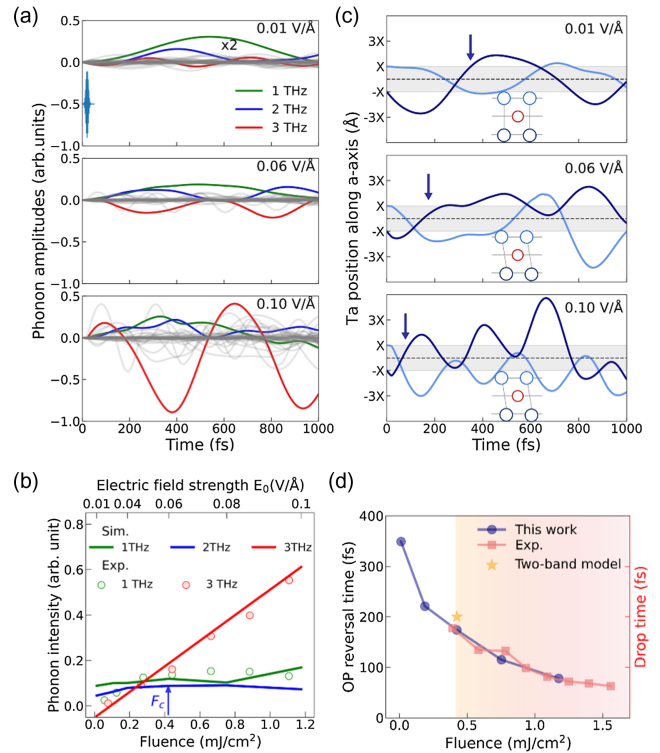


FIG. 2. (a) Time-dependent phonon excitations under different laser strength  $E_0$ . The gray lines present the intensities for the rest of 45 phonon modes, excluding those at 1, 2, and 3 THz. (b) Laser fluence dependence of three dominant phonon modes. To match the experimental data reproduced from Refs. [19,21], the simulated fluence was rescaled by calibrating the threshold fluence of the 1 THz mode ( $\sim 0.38 \text{ mJ/cm}^2$ ), by assuming a refractive index of  $n = 2$ . Here,  $F_c \approx 0.42 \text{ mJ/cm}^2$  denotes the laser fluence threshold of the 2 THz mode. (c) Real-time positions of two adjacent Ta chains along the  $a$  axis. The arrow in each panel denotes the time for the lattice OP reversal. (d) Time constant of lattice OP reversal compared with the two-band model prediction (Ref. [19]) and the experimental measurement of the drop time for the spectral weight of the top valence band, indicating the IMT (Ref. [29]). The colored region represents the fluence range that enables long-term OP reversal ( $F > F_c$ ).

(TDDFT-MD) simulations were conducted, using the primitive cell of  $\text{Ta}_2\text{NiSe}_5$  with the fixed monoclinic lattice. The rationality of this setup is supported by recent experimental observations indicating that the lattice symmetry of the sample remains stable even when subjected to intense laser illumination [17,28,32,33]. Laser pulses polarized along the  $a$  axis were applied with varying strength ( $E_0$ ) and the wavelength is 800 nm ( $\hbar\omega = 1.55 \text{ eV}$ ) (for details see note S1 in the Supplemental Material [34] and Refs. [35–45] therein).

Figure 2 illustrates the results of the TDDFT-MD simulations, focusing on the dynamics of lattice structure. The time evolution of each phonon branch is obtained by projecting the displacement of ions onto the phonon eigenvectors calculated from the equilibrium ground state [46,47].

The amplitudes of the excited phonons accurately reproduce the measurement from experiments [21,33]. Notably, the phonon coupled to the EI, such as 1 and 2 THz modes, exhibit sensitivity to laser excitation due to exciton depletion. Beyond certain laser fluence thresholds, the amplitude growth of these modes reaches a saturation point. This observation, along with the subsequent exploration of carrier dynamics, results in the determination of  $F_c \approx 0.38$  and  $0.42$  mJ/cm<sup>2</sup> for the 1 and 2 THz modes, respectively [34]. Among the uncoupled coherent phonons, the displacive excitation of 3 THz mode is particularly prominent and shows a linear dependence on  $F$  [Figs. 2(a) and 2(b)].

In practice, the phase insensitivity of pump-probe techniques has posed a limitation on the detailed analysis of atomic configurations in thermally inaccessible metallic states [24,29,30,33,45,48,49]. Here, we show that the new energy minimum of the excited states shifts towards the positive (negative) direction of the calculated eigenvector of the 2 THz (3 THz) mode (Fig. S1 [34]). This means that the displacements of Ta ions lead to the reversal of the lattice OP along the  $a$  axis and an enlarged Ta-Ni distance along the  $c$  axis. These unidirectional movements can be attributed to the asymmetrical deformation of the PES upon excitation of the two phonon modes [Fig. 3(c)]. In contrast, when the rest of the coherent phonons are excited, they only drive harmonic oscillations around the equilibrium position with small amplitude.

The OP reversal of the lattice subsystem is further confirmed by monitoring the real-time positions of the ions [Fig. 2(c)]. Under weak field conditions (e.g.,  $E_0 = 0.01$  V/Å), the new equilibrium positions resemble that in the orthorhombic phase, where the shear displacement between two adjacent Ta chains vanishes, resulting in the quasiequilibrium OP transitioning from  $X$  to  $0$ . This can be explained by that the tiny energy barrier ( $\sim 6$  meV per formula unit) between the two atomic configurations has been provided by the laser pumping. The transient OP reversal occurs at 350 fs, with an oscillating frequency of 2 THz, consistent with previous frequency-domain ARPES studies indicating that this mode is highly relevant to the emergence of photoinduced semi-metallic states [18,48].

Long-term order parameter inversion occurs upon reaching  $F_c$  of the 2 THz mode ( $E_0 = 0.06$  V/Å), resulting in a metastable metallic state. In this state, the two Ta chains exchange their positions along the shear motion direction, while the intermediate Ni chain experiences minor oscillations around its ground-state equilibrium position [Fig. 1(d) and Fig. S2 [34]]. As the laser amplitude is further increased (e.g.,  $E_0 = 0.1$  V/Å), the stability of the metastable state is enhanced, resulting in a longer lifetime  $\sim 600$  fs (note S2 and Fig. S3) [34]. Meanwhile, the oscillation frequency changes to larger values ( $\sim 4$  THz), indicating modulation of the landscape of PES.

The time constant of lattice OP reversal is approximately inversely dependent on the laser amplitude  $E_0$  (Fig. S4 [34]),

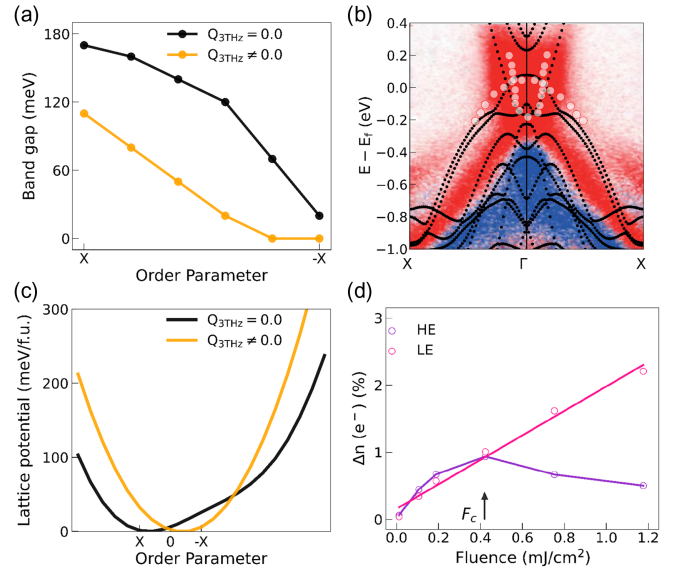


FIG. 3. (a) The dependence of band gap on lattice order parameter under two conditions: One with a finite structural distortion induced by the 3 THz mode excitation ( $Q_{3\text{THz}} = 0.007$  Å amu<sup>1/2</sup>) and the other with  $Q_{3\text{THz}} = 0$ . (b) Band structure of the transient metallic state when  $E_0 = 0.06$  V/Å,  $t = 200$  fs (black dots). The colored plots represent ARPES spectra, and the white dots are the corresponding theoretical fitting, both reproduced from Ref. [18]. (c) Potential energy profile along the lattice OP reversal pathway with or without finite structural distortion induced by the 3 THz mode excitation ( $Q_{3\text{THz}} = 0.04$  Å amu<sup>1/2</sup>). For comparison, the minimum energy of each curve is set as 0. (d) Percentage of excited electrons from two energy ranges of VBs as a function of laser fluence. LE: from deep VBs ( $-1.35 \leq E_{\text{VB}} - E_F \leq -0.85$  eV) to low-energy CBs ( $0.2 \leq E_{\text{CB}} - E_F \leq 0.7$  eV); HE: from top VBs ( $-0.5 \leq E_{\text{VB}} - E_F \leq 0$  eV) to high-energy CBs ( $1.05 \leq E_{\text{CB}} - E_F \leq 1.55$  eV).

which is similar to the trend in gap quenching [29] [Fig. 2(d)]. This alignment between the simulated and measured time constants could potentially be coincidental, arising from the complex interplay of diverse variables that compensate for each other. Nevertheless, meticulous measures have been implemented to bolster the reliability of this qualitative comparison (note S3 [34]). It suggests that the observed metallic phase could be a result of the modulated electronic structure due to coherent lattice displacements, at least, it is not a purely electronic process. This finding is aligned with the theoretical demonstration that electronically driven EI phase is highly susceptible to even small atomic distortions and can be only realized within a narrow parameter space of on-site and intersite Coulomb interactions [6,50].

Besides the dominant role of the 2 THz mode, coherent excitation of the 3 THz mode is vital in driving the complete gap collapse. Figure 3(a) shows the evolution of band gap based on the  $G_0W_0$  method (Fig. S5 [34]), which incorporates many-body corrections to achieve a quantitative agreement with experimental measurements [51,52]. The initial state presents a band gap of 170 meV in the  $G_0W_0$

calculation, agreeing with the measured optical gap of 160 meV [53]. The gap narrows and reaches its minimum value of 20 meV when the lattice OP is solely reversed. Only when finite atomic displacements along the eigenvector of the 3 THz mode are superimposed, the gap is completely quenched. Since the quasiparticle gap originates from the putative excitonic condensation, its decrease and eventual disappearance indicate the depletion of excitons [19,21,24,53].

The dynamical IMT is further confirmed by monitoring the time-dependent band structure of  $\text{Ta}_2\text{NiSe}_5$ . Figure 3(b) shows the comparison between the simulated results obtained when the metastable metallic state is achieved and the tr-ARPES measurements under a strong pump field ( $2.27 \text{ mJ/cm}^2$ ). The experimental features of IMT are well produced, including the upward shift of the hole bands, the downward shift of the electron bands, and their crossing of the Fermi level at the same wave vector [18,29]. The density of states (DOS) around the  $E_F$  increases with the larger atomic distortion induced by the 3 THz mode (Fig. S6 [34]), consistent with the observed drop in resistivity following intense excitations [45]. Therefore, the atomic configuration of the experimentally detected metallic states [45,49] has been clarified, as shown in Fig. 1(e).

To understand the cooperative interactions between the two modes, which are commonly disregarded [16,23,54,55], the potential energy profile along the lattice OP reversal pathway is shown in Fig. 3(c). It is evident that finite structural distortion induced by the excitation of the 3 THz mode tends to shift the energy minimum from the ground-state atomic configuration to its OP reversal counterpart. The curvature of the modulated PES increases with larger phonon amplitudes (Fig. S7 [34]), indicating that a higher energy barrier needs to be overcome to escape from the new energy minimum position, which enables the stability of reversed OP under strong fields. It implies that the anharmonic coupling between the two modes, leads to a new nonequilibrium combination mode [56,57], whose eigenvector consists of fixed atomic displacements (leading to the OP reversal) and tunable atomic displacements along the eigenvectors of the 2 and 3 THz modes, respectively. Additional evidence supporting the strong anharmonic coupling comes from the fact that oscillation frequencies of these two modes converge toward each other under the strong fields (note S4 and Fig. S8 in Ref. [34]).

The excitation and coupling of the two optical phonons are closely related to the charge dynamics, due to the strong EPC. Previous studies have indicated that the 2 THz mode is excited by hole (electron) occupation on top of valence bands (VBs) [high-energy conduction bands (CBs)], and the saturation threshold is attributed to the absorption saturation of pump photons near the Gamma point [22]. By tracking the momentum-resolved carrier distribution after laser illumination (Fig. S9 [34]), we have verified the validity of these statements and we further demonstrate that

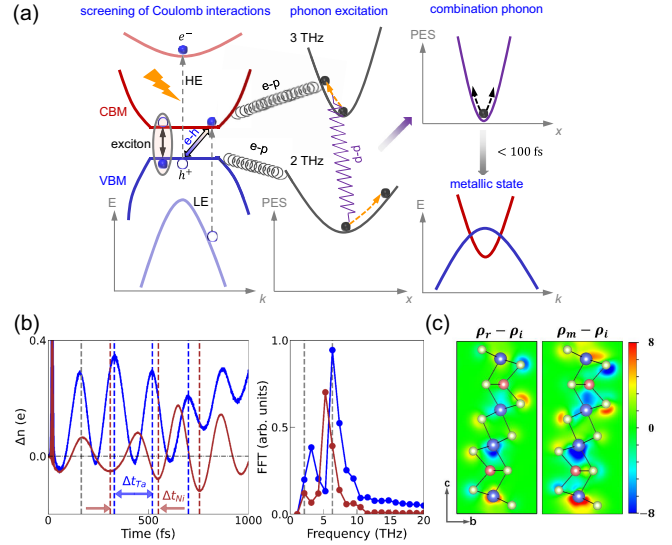


FIG. 4. (a) The schematic for the photoinduced ultrafast exciton-phonon dynamic in  $\text{Ta}_2\text{NiSe}_5$ . Here, the electron-hole, electron-phonon, and phonon-phonon interactions are abbreviated as e-h, e-p, and p-p, respectively. (b) The effective charge of Ta and Ni over time, along with their Fourier transformations when  $E_0 = 0.08 \text{ V/\AA}$ . Here,  $\Delta t_{\text{Ta}}$  and  $\Delta t_{\text{Ni}}$  denote the time intervals between two consecutive oscillation cycles of Ta and Ni elements, with  $\Delta t_{\text{Ta}} < \Delta t_{\text{Ni}}$ . Gray dashed lines in the Fourier transform spectrum are used to mark the peak positions of the predominant carrier oscillations, approximately around 2 and 6 THz. (c) Charge density differences between the lattice OP reversal state ( $\rho_r$ ) and initial state ( $\rho_i$ ), as well as between the metallic state ( $\rho_m$ ) and initial state. The unit of charge density differences is  $10^{-3} e a_0^{-3}$ ,  $a_0$  is the Bohr radius. The red (blue) region represents the increase (decrease) in charge density.

the 3 THz mode is strongly coupled with the electronic excitation from deep VBs to the bottom of CBs, by analyzing the forces applied to ions with fixed carrier occupation (Fig. S10 [34]). The linear and saturation behavior of electronic depopulation in deep and top VBs, respectively, are consistent with the amplitude evolution of the excited 3 and 2 THz modes (Fig. 3(d) and note S5 [34]). Therefore, it can be inferred that the interactions between excited holes (electrons) occupying the VB maximum (VBM) [CB minimum (CBM)] enable the coupling between the two phonons. This explanation also consistent with the tr-ARPES observations that these two modes have the most remarkable responses around  $E_F$  [17,18,32,33].

The comprehensive understanding of exciton-phonon dynamics [12,13] during the IMT is summarized in Fig. 4(a). Upon photoexcitation, the excitonic effect, which is the formation of bound electron-hole pairs, is weakened due to the screening of Coulomb interactions by photocarriers [4]. The induced modulation of the electronic structure is accelerated with a higher density of photocarriers, leading to stronger phonon excitations due to EPC. The emergence of a

nonequilibrium mode up-conversion, arising from anharmonic phonon interactions, reshapes the PES. This modulation of the PES enables the rapid metallization and lattice OP reversal within a timescale of 100 fs or faster. The timescales are comparable to purely electronic processes and, in turn, facilitate the destabilization of EI phase [24].

These findings address the fundamental questions about why picosecond timescale phonon excitations could dominate the excitonic quenching [17,21,45,58] and, shed light on the structural origin of ultrafast insulator-to-metal transitions. What sets this work apart is its ability to disentangle different order parameters simultaneously in the time domain, a distinctive feature when compared to recent literature. Most prominent papers focusing on the ultrafast response of Ta<sub>2</sub>NiSe<sub>5</sub> do not delve into non-equilibrium many-body interactions [29,45,49]. While a few latest articles have conducted EPC analysis, their focus has predominantly centered on establishing correlations between excited phonon amplitude and laser parameters [14,24], as well as investigating the impact of individual phonon modes on the ground-state electronic structure [50]. This study goes beyond these limitations by revealing the intricate characteristics of thermally inaccessible metallic states, which are challenging to be discerned solely through experimental approaches or speculative models.

Based on our simulations, we propose two strategies for the further pump-probe investigations to elucidate the explicit role of electronic correlations. (i) Employ an ultrashort extreme ultraviolet (XUV) pulse with a sub-10 fs duration as the probe pulse. It enables real-time monitoring of transient electronic structure with high temporal resolution, albeit potentially at the cost of lower energy resolution. This approach allows for assessing gap closure with an ultimate response time of  $\sim 10$  fs while investigating its correlation with a  $F^{-0.5}$  relationship, indicative of purely electronic processes [59,60]. (ii) Utilize weak pump pulses below the reported fluence threshold ( $F_c$ ) but still sufficiently strong to disrupt electronic correlations [19,33]. This strategy effectively minimizes the impact of structural distortion, with any potential gap collapse due to structural instability occurring at significantly longer time constants ( $>100$  fs). Lower temporal resolution in this scenario remains sufficient, enhancing energy resolution for precise gap dynamics measurements. The observation of a phase transition within 100 fs under these conditions strongly supports the primary role of electronic correlations.

Because of the limitations of the (semi)local exchange-correlation (e.g., PBE) functional in rt-TDDFT calculations, the accurate description of excitons is challenging. Here, the possible exciton-related dynamics were inferred by analyzing the collective oscillation of carriers between Ta and Ni chains. Laser irradiation has the most significant effect on the effective charge of Ta and Se atoms, ca., increase by 0.26 e and decrease by 0.3 e in the period after

the laser action (Fig. S12 [34]). The charge transfer induces strong ion-ion interactions, which account for the distortion of Ta-Se octahedra and the enlarged distance between Ta and Ni chains right after photoexcitation. Beyond the threshold fluence  $F_c$ , the desynchronization of electron and hole oscillations becomes evident through distinct oscillation frequencies in charge evolution at Ta and Ni ions, signaling exciton destabilization [Fig. 4(b)]. For comparison, under weak fields, nearly synchronous charge oscillations with similar frequencies remain well preserved [Note S6 and Fig. S13]. Therefore, the rt-TDDFT quantum dynamics simulations already capture the most significant physics and experimental features [21,24].

In conclusion, we have unraveled structural origin of insulator-to-metal phase transition and the significance of non-equilibrium interactions between the EI-OP-coupled and regular-coherent phonons. A comprehensive picture about the nature of photoinduced exciton-phonon dynamics is provided, and the simulated IMT timescales and spectral features agree well with the available experimental data, suggesting the reinforced relevance between phonon dynamics and low-energy electronic structure. Our study provides a unique perspective towards understanding the mechanism of IMT in Ta<sub>2</sub>NiSe<sub>5</sub> and hints for new pathways for its manipulation.

S. M. acknowledges partial financial support from the National Key Research and Development Program of China (No. 2021YFA1400201), National Natural Science Foundation of China (No. 11934003 and No. 12025407), and “Strategic Priority Research Program (B)” of the Chinese Academy of Sciences (No. XDB33030100 and No. YSBR-047). Y.-G. Y. acknowledges partial financial support from the National Key Research and Development Program of China (No. 2020YFA0308800), National Natural Science Foundation of China (No. 12061131002 and No. 12234003). M.-X. G. acknowledges support from the National Natural Science Foundation of China (Grant No. 12304536) and the start-up funding of Beijing Institute of Technology. The authors acknowledge helpful discussions with Professor Dao Xiang.

\*Corresponding author: ygyao@bit.edu.cn

†Corresponding author: smeng@iphy.ac.cn

- [1] S. Safaei and D. A. Mazziotti, Quantum signature of exciton condensation, *Phys. Rev. B* **98**, 045122 (2018).
- [2] Y. Wakisaka, T. Sudo, K. Takubo, T. Mizokawa, M. Arita, H. Namatame, M. Taniguchi, N. Katayama, M. Nohara, and H. Takagi, Excitonic insulator state in Ta<sub>2</sub>NiSe<sub>5</sub> probed by photoemission spectroscopy, *Phys. Rev. Lett.* **103**, 026402 (2009).
- [3] K. Seki *et al.*, Excitonic Bose-Einstein condensation in Ta<sub>2</sub>NiSe<sub>5</sub> above room temperature, *Phys. Rev. B* **90**, 155116 (2014).

- [4] K. Sugimoto, S. Nishimoto, T. Kaneko, and Y. Ohta, Strong coupling nature of the excitonic insulator state in Ta<sub>2</sub>NiSe<sub>5</sub>, *Phys. Rev. Lett.* **120**, 247602 (2018).
- [5] T. Kaneko, T. Toriyama, T. Konishi, and Y. Ohta, Orthorhombic-to-monoclinic phase transition of Ta<sub>2</sub>NiSe<sub>5</sub> induced by the Bose-Einstein condensation of excitons, *Phys. Rev. B* **87**, 035121 (2013).
- [6] G. Mazza, M. Rosner, L. Windgatter, S. Latini, H. Hubener, A. J. Millis, A. Rubio, and A. Georges, Nature of symmetry breaking at the excitonic insulator transition: Ta<sub>2</sub>NiSe<sub>5</sub>, *Phys. Rev. Lett.* **124**, 197601 (2020).
- [7] A. Nakano, T. Hasegawa, S. Tamura, N. Katayama, S. Tsutsui, and H. Sawa, Antiferroelectric distortion with anomalous phonon softening in the excitonic insulator Ta<sub>2</sub>NiSe<sub>5</sub>, *Phys. Rev. B* **98**, 045139 (2018).
- [8] M. D. Watson, I. Marković, E. A. Morales, P. Le Fèvre, M. Merz, A. A. Haghighirad, and P. D. C. King, Band hybridization at the semimetal-semiconductor transition of Ta<sub>2</sub>NiSe<sub>5</sub> enabled by mirror-symmetry breaking, *Phys. Rev. Res.* **2**, 013236 (2020).
- [9] M.-J. Kim, A. Schulz, T. Takayama, M. Isobe, H. Takagi, and S. Kaiser, Phononic soft mode behavior and a strong electronic background across the structural phase transition in the excitonic insulator Ta<sub>2</sub>NiSe<sub>5</sub>, *Phys. Rev. Res.* **2**, 042039(R) (2020).
- [10] A. Subedi, Orthorhombic-to-monoclinic transition in Ta<sub>2</sub>NiSe<sub>5</sub> due to a zone-center optical phonon instability, *Phys. Rev. Mater.* **4**, 083601 (2020).
- [11] F. J. Di Salvo, C. H. Chen, R. M. Fleming, J. V. Waszczak, R. G. Dunn, S. A. Sunshine, and J. A. Ibers, Physical and structural properties of the new layered compounds Ta<sub>2</sub>NiS<sub>5</sub> and Ta<sub>2</sub>NiSe<sub>5</sub>, *J. Less Common Metals* **116**, 51 (1986).
- [12] T. I. Larkin, R. D. Dawson, M. Höppner, T. Takayama, M. Isobe, Y. L. Mathis, H. Takagi, B. Keimer, and A. V. Boris, Infrared phonon spectra of quasi-one-dimensional Ta<sub>2</sub>NiSe<sub>5</sub> and Ta<sub>2</sub>NiS<sub>5</sub>, *Phys. Rev. B* **98**, 125113 (2018).
- [13] T. I. Larkin *et al.*, Giant exciton Fano resonance in quasi-one-dimensional Ta<sub>2</sub>NiSe<sub>5</sub>, *Phys. Rev. B* **95**, 195144 (2017).
- [14] K. Kim, H. Kim, J. Kim, C. Kwon, J. S. Kim, and B. J. Kim, Direct observation of excitonic instability in Ta<sub>2</sub>NiSe<sub>5</sub>, *Nat. Commun.* **12**, 1969 (2021).
- [15] P. A. Volkov, M. Ye, H. Lohani, I. Feldman, A. Kanigel, and G. Blumberg, Critical charge fluctuations and emergent coherence in a strongly correlated excitonic insulator, *npj Quantum Mater.* **6**, 52 (2021).
- [16] Y. Murakami, D. Golež, T. Kaneko, A. Koga, A. J. Millis, and P. Werner, Collective modes in excitonic insulators: Effects of electron-phonon coupling and signatures in the optical response, *Phys. Rev. B* **101**, 195118 (2020).
- [17] E. Baldini *et al.*, The spontaneous symmetry breaking in Ta<sub>2</sub>NiSe<sub>5</sub> is structural in nature, *Proc. Natl. Acad. Sci. U.S.A.* **120**, e2221688120 (2023).
- [18] T. Suzuki, Y. Shinohara, Y. Lu, M. Watanabe, J. Xu *et al.*, Detecting electron-phonon coupling during photoinduced phase transition, *Phys. Rev. B* **103**, L121105 (2021).
- [19] H. Ning, O. Mehio, M. Buchhold, T. Kurumaji, G. Refael, J. G. Checkelsky, and D. Hsieh, Signatures of ultrafast reversal of excitonic order in Ta<sub>2</sub>NiSe<sub>5</sub>, *Phys. Rev. Lett.* **125**, 267602 (2020).
- [20] J. C. Petersen *et al.*, Clocking the melting transition of charge and lattice order in 1T-TaS<sub>2</sub> with ultrafast extreme-ultraviolet angle-resolved photoemission spectroscopy, *Phys. Rev. Lett.* **107**, 177402 (2011).
- [21] D. Werdehausen, T. Takayama, M. Höppner, G. Albrecht, A. W. Rost, Y. Lu, D. Manske, H. Takagi, and S. Kaiser, Coherent order parameter oscillations in the ground state of the excitonic insulator Ta<sub>2</sub>NiSe<sub>5</sub>, *Sci. Adv.* **4**, eaap8652 (2018).
- [22] S. Mor *et al.*, Ultrafast electronic band gap control in an excitonic insulator, *Phys. Rev. Lett.* **119**, 086401 (2017).
- [23] H. M. Bretscher *et al.*, Imaging the coherent propagation of collective modes in the excitonic insulator Ta<sub>2</sub>NiSe<sub>5</sub> at room temperature, *Sci. Adv.* **7**, eabd6147 (2021).
- [24] H. M. Bretscher, P. Andrich, P. Telang, A. Singh, L. Harnagea, A. K. Sood, and A. Rao, Ultrafast melting and recovery of collective order in the excitonic insulator Ta<sub>2</sub>NiSe<sub>5</sub>, *Nat. Commun.* **12**, 1699 (2021).
- [25] H. Jog, L. Harnagea, E. J. Mele, and R. Agarwal, Exchange coupling mediated broken symmetries in Ta<sub>2</sub>NiSe<sub>5</sub> revealed from quadrupolar circular photogalvanic effect, *Sci. Adv.* **8**, eabl9020 (2022).
- [26] K. Fukutani, R. Stania, C. Il Kwon, J. S. Kim, K. J. Kong, J. Kim, and H. W. Yeom, Detecting photoelectrons from spontaneously formed excitons, *Nat. Phys.* **17**, 1024 (2021).
- [27] D. Golež, S. K. Y. Dufresne, M.-J. Kim, F. Boschini, H. Chu *et al.*, Unveiling the underlying interactions in Ta<sub>2</sub>NiSe<sub>5</sub> from photoinduced lifetime change, *Phys. Rev. B* **106**, L121106 (2022).
- [28] K. Katsumi, A. Alekhin, S.-M. Souliou, M. Merz, A.-A. Haghighirad, M. Le Tacon, S. Houver, M. Cazayous, A. Sacuto, and Y. Gallais, Disentangling lattice and electronic instabilities in the excitonic insulator candidate Ta<sub>2</sub>NiSe<sub>5</sub> by nonequilibrium spectroscopy, *Phys. Rev. Lett.* **130**, 106904 (2023).
- [29] K. Okazaki *et al.*, Photo-induced semimetallic states realised in electron-hole coupled insulators, *Nat. Commun.* **9**, 4322 (2018).
- [30] T. Saha, D. Golež, G. De Ninno, J. Mravlje, Y. Murakami, B. Ressel, M. Stupar, and P. R. Ribič, Photoinduced phase transition and associated timescales in the excitonic insulator Ta<sub>2</sub>NiSe<sub>5</sub>, *Phys. Rev. B* **103**, 144304 (2021).
- [31] F. Krausz and M. Ivanov, Attosecond physics, *Rev. Mod. Phys.* **81**, 163 (2009).
- [32] S. Mor, M. Herzog, J. Noack, N. Katayama, M. Nohara, H. Takagi, A. Trunschke, T. Mizokawa, C. Monney, and J. Stähler, Inhibition of the photoinduced structural phase transition in the excitonic insulator Ta<sub>2</sub>NiSe<sub>5</sub>, *Phys. Rev. B* **97**, 115154 (2018).
- [33] T. Tang, H. Wang, S. Duan, Y. Yang, C. Huang, Y. Guo, D. Qian, and W. Zhang, Non-Coulomb strong electron-hole binding in Ta<sub>2</sub>NiSe<sub>5</sub> revealed by time- and angle-resolved photoemission spectroscopy, *Phys. Rev. B* **101**, 235148 (2020).
- [34] See Supplemental Material at <http://link.aps.org/supplemental/10.1103/PhysRevLett.131.256503> for details about the theoretical methods and other discussion.
- [35] G. Kresse and J. Furthmüller, Efficiency of *ab initio* total energy calculations for metals and semiconductors using a plane-wave basis set, *Comput. Mater. Sci.* **6**, 15 (1996).

- [36] G. Kresse and J. Furthmüller, Efficient iterative schemes for *ab initio* total-energy calculations using a plane-wave basis set, *Phys. Rev. B* **54**, 11169 (1996).
- [37] G. Kresse and D. Joubert, From ultrasoft pseudopotentials to the projector augmented-wave method, *Phys. Rev. B* **59**, 1758 (1999).
- [38] A. Togo and I. Tanaka, First principles phonon calculations in materials science, *Scr. Mater.* **108**, 1 (2015).
- [39] J. P. Perdew, K. Burke, and M. Ernzerhof, Generalized gradient approximation made simple, *Phys. Rev. Lett.* **77**, 3865 (1996).
- [40] A. Nakano *et al.*, Pressure-induced coherent sliding-layer transition in the excitonic insulator Ta<sub>2</sub>NiSe<sub>5</sub>, *Int. Union Crystallogr. J.* **5**, 158 (2018).
- [41] C. Lian, M. Guan, S. Hu, J. Zhang, and S. Meng, Photoexcitation in solids: First-principles quantum simulations by real-time TDDFT, *Adv. Theory. Simul.* **1**, 1800055 (2018).
- [42] M. Guan, D. Chen, S. Hu, H. Zhao, P. You, and S. Meng, Theoretical insights into ultrafast dynamics in quantum materials, *Ultrafast Sci.* **2022**, 9767251 (2022).
- [43] Y. C. Tian *et al.*, Ultrafast dynamics evidence of high temperature superconductivity in single unit cell FeSe on SrTiO<sub>3</sub>, *Phys. Rev. Lett.* **116**, 107001 (2016).
- [44] A. Boyer, M. Hervé, V. Despré, P. Castellanos Nash, V. Lorient, A. Marciniak, A. G. G. M. Tielens, A. I. Kuleff, and F. Lépine, Ultrafast vibrational relaxation dynamics in XUV-excited polycyclic aromatic hydrocarbon molecules, *Phys. Rev. X* **11**, 041012 (2021).
- [45] Q. M. Liu *et al.*, Photoinduced multistage phase transitions in Ta<sub>2</sub>NiSe<sub>5</sub>, *Nat. Commun.* **12**, 2050 (2021).
- [46] M.-X. Guan, X.-B. Liu, D.-Q. Chen, X.-Y. Li, Y.-P. Qi, Q. Yang, P.-W. You, and S. Meng, Optical control of multistage phase transition via phonon coupling in MoTe<sub>2</sub>, *Phys. Rev. Lett.* **128**, 015702 (2022).
- [47] C. Song, Q. Yang, X. Liu, H. Zhao, C. Zhang, and S. Meng, Electronic origin of laser-induced ferroelectricity in SrTiO<sub>3</sub>, *J. Phys. Chem. Lett.* **14**, 576 (2023).
- [48] T. Miyamoto *et al.*, Charge and lattice dynamics in excitonic insulator Ta<sub>2</sub>NiSe<sub>5</sub> investigated using ultrafast reflection spectroscopy, *J. Phys. Soc. Jpn.* **91**, 023701 (2022).
- [49] K. Katsumi, A. Alekhin, S.-M. Souliou, M. Merz, A.-A. Haghighirad, M. Le Tacon, S. Houver, M. Cazayous, A. Sacuto, and Y. Gallais, Disentangling lattice and electronic instabilities in the excitonic insulator candidate Ta<sub>2</sub>NiSe<sub>5</sub> by nonequilibrium spectroscopy, *Phys. Rev. Lett.* **130**, 106904 (2023).
- [50] L. Windgätter, M. Rösner, G. Mazza, H. Hübener, A. Georges, A. J. Millis, S. Latini, and A. Rubio, Common microscopic origin of the phase transitions in Ta<sub>2</sub>NiS<sub>5</sub> and the excitonic insulator candidate Ta<sub>2</sub>NiSe<sub>5</sub>, *npj Comput. Mater.* **7**, 210 (2021).
- [51] M. van Schilfhaarde, T. Kotani, and S. Faleev, Quasiparticle self-consistent GW theory, *Phys. Rev. Lett.* **96**, 226402 (2006).
- [52] M. S. Hybertsen and S. G. Louie, First-principles theory of quasiparticles: Calculation of band gaps in semiconductors and insulators, *Phys. Rev. Lett.* **55**, 1418 (1985).
- [53] Y. F. Lu, H. Kono, T. I. Larkin, A. W. Rost, T. Takayama, A. V. Boris, B. Keimer, and H. Takagi, Zero-gap semiconductor to excitonic insulator transition in Ta<sub>2</sub>NiSe<sub>5</sub>, *Nat. Commun.* **8**, 14408 (2017).
- [54] B. Remez and N. R. Cooper, Effects of disorder on the transport of collective modes in an excitonic condensate, *Phys. Rev. B* **101**, 235129 (2020).
- [55] D. Golez, Z. Sun, Y. Murakami, A. Georges, and A. J. Millis, Nonlinear spectroscopy of collective modes in an excitonic insulator, *Phys. Rev. Lett.* **125**, 257601 (2020).
- [56] H. Siegle, G. Kaczmarczyk, L. Filippidis, A. P. Litvinchuk, A. Hoffmann, and C. Thomsen, Zone-boundary phonons in hexagonal and cubic GaN, *Phys. Rev. B* **55**, 7000 (1997).
- [57] Y. Yin, A. G. Walsh, A. N. Vamivakas, S. B. Cronin, D. E. Prober, and B. B. Goldberg, Electron-phonon coupling of Gmode and assignment of a combination mode in carbon nanotubes, *Phys. Rev. B* **84**, 075428 (2011).
- [58] S. Duan, W. Xia, C. Huang, S. Wang, L. Gu, H. Liu, D. Xiang, D. Qian, Y. Guo, and W. Zhang, Ultrafast switching from the charge density wave phase to a metastable metallic state in 1T - TiSe<sub>2</sub>, *Phys. Rev. Lett.* **130**, 226501 (2023).
- [59] D. N. Basov, R. D. Averitt, D. van der Marel, M. Dressel, and K. Haule, Electrodynamics of correlated electron materials, *Rev. Mod. Phys.* **83**, 471 (2011).
- [60] T. Rohwer *et al.*, Collapse of long-range charge order tracked by time-resolved photoemission at high momenta, *Nature (London)* **471**, 490 (2011).